Molecular Cell, Volume *53*

Supplemental Information

Dimeric Structure of Pseudokinase RNase L Bound to 2-5A Reveals a Basis for Interferon-Induced Antiviral Activity

Hao Huang, Elton Zeqiraj, Beihua Dong, Babal Kant Jha, Nicole M. Duffy, Stephen Orlicky, Neroshan Thevakumaran, Manisha Talukdar, Monica C. Pillon, Derek F. Ceccarelli, Leo C.K. Wan, Yu-Chi Juang, Daniel Y.L. Mao, Christina Gaughan, Margo A. Brinton, Andrey A. Perelygin, Igor Kourinov, Alba Guarné, Robert H. Silverman, and Frank Sicheri

Supplementary Information Inventory

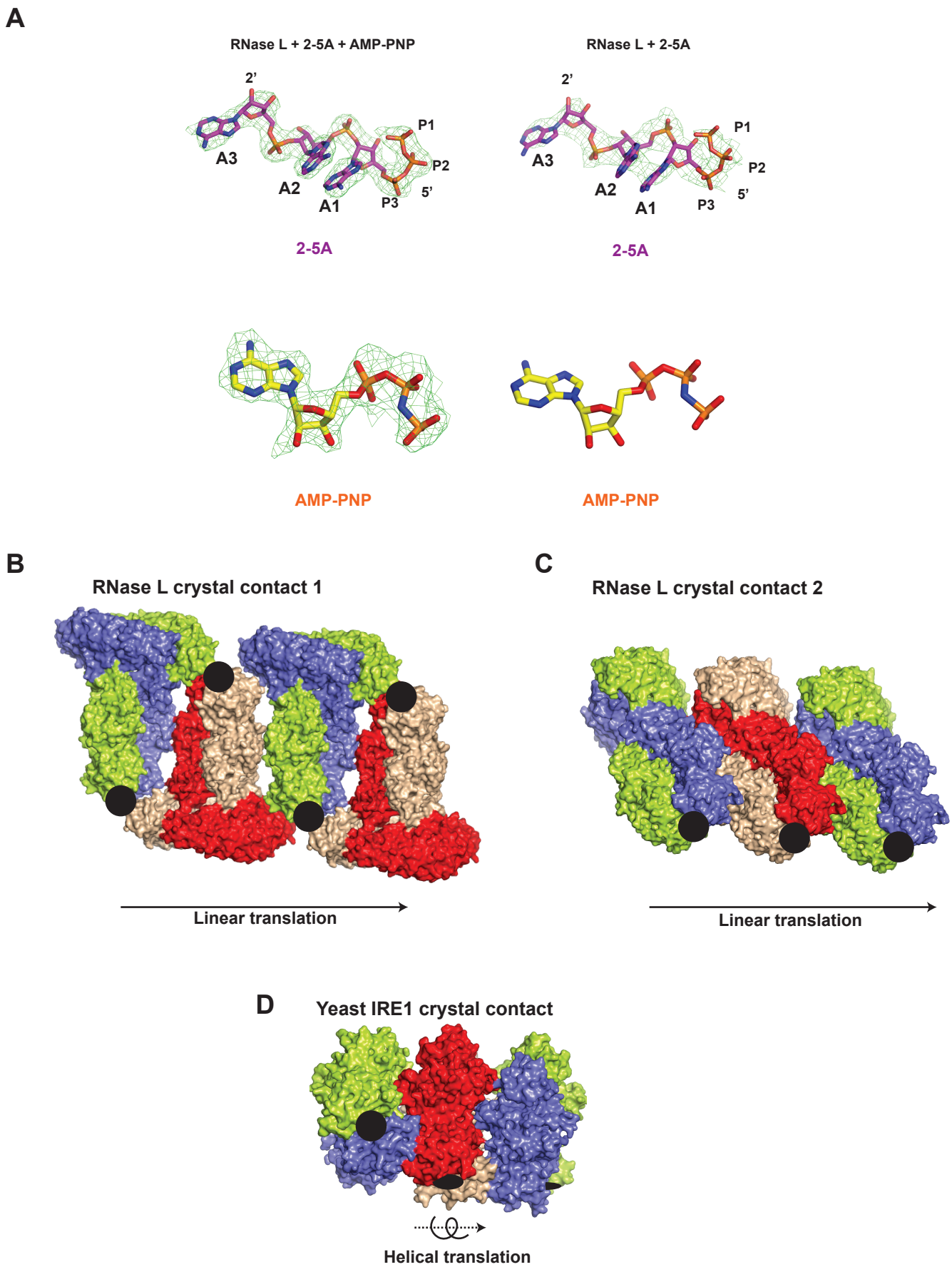

Supplementary Figure 1

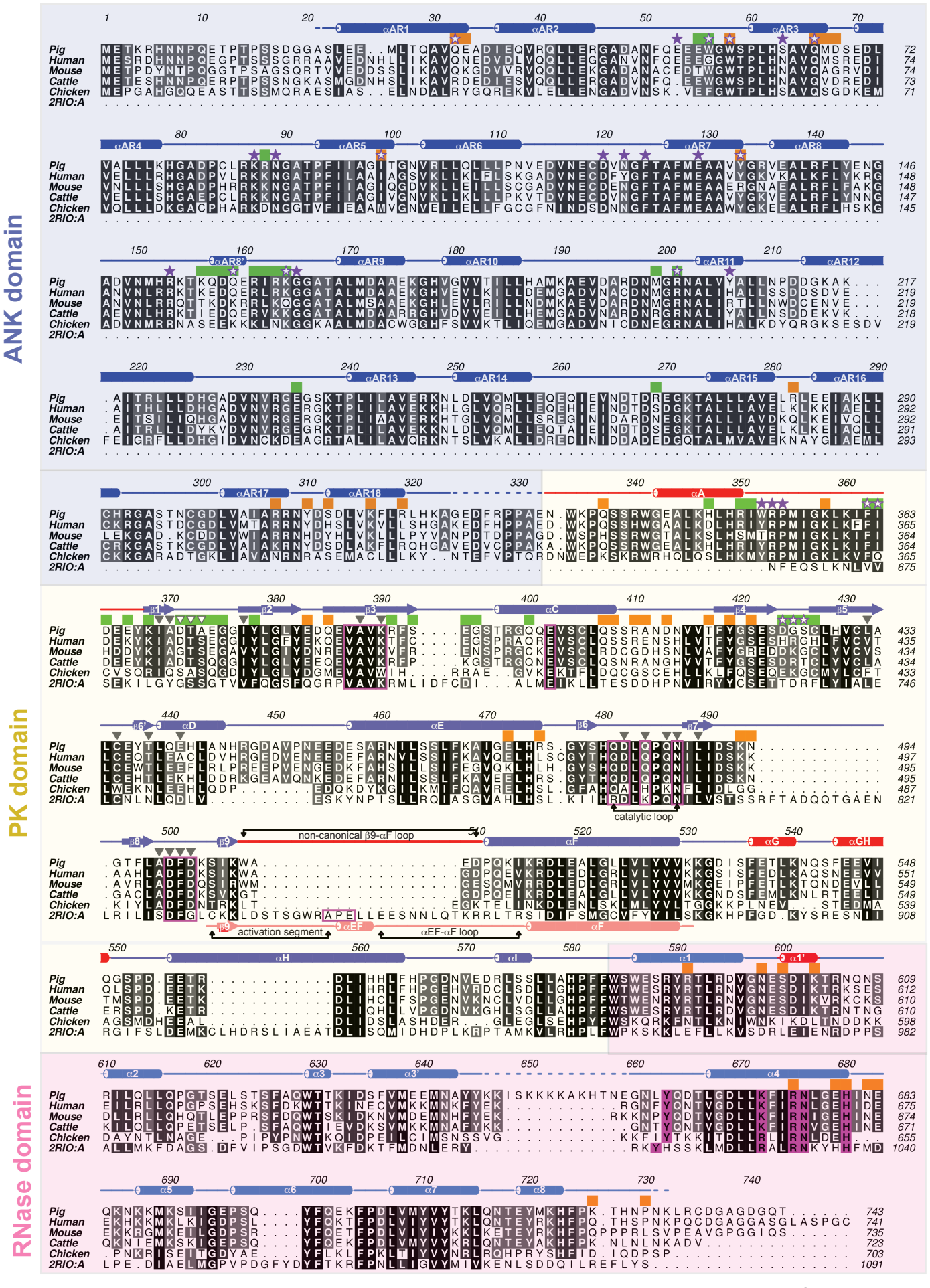

Supplementary Figure 2

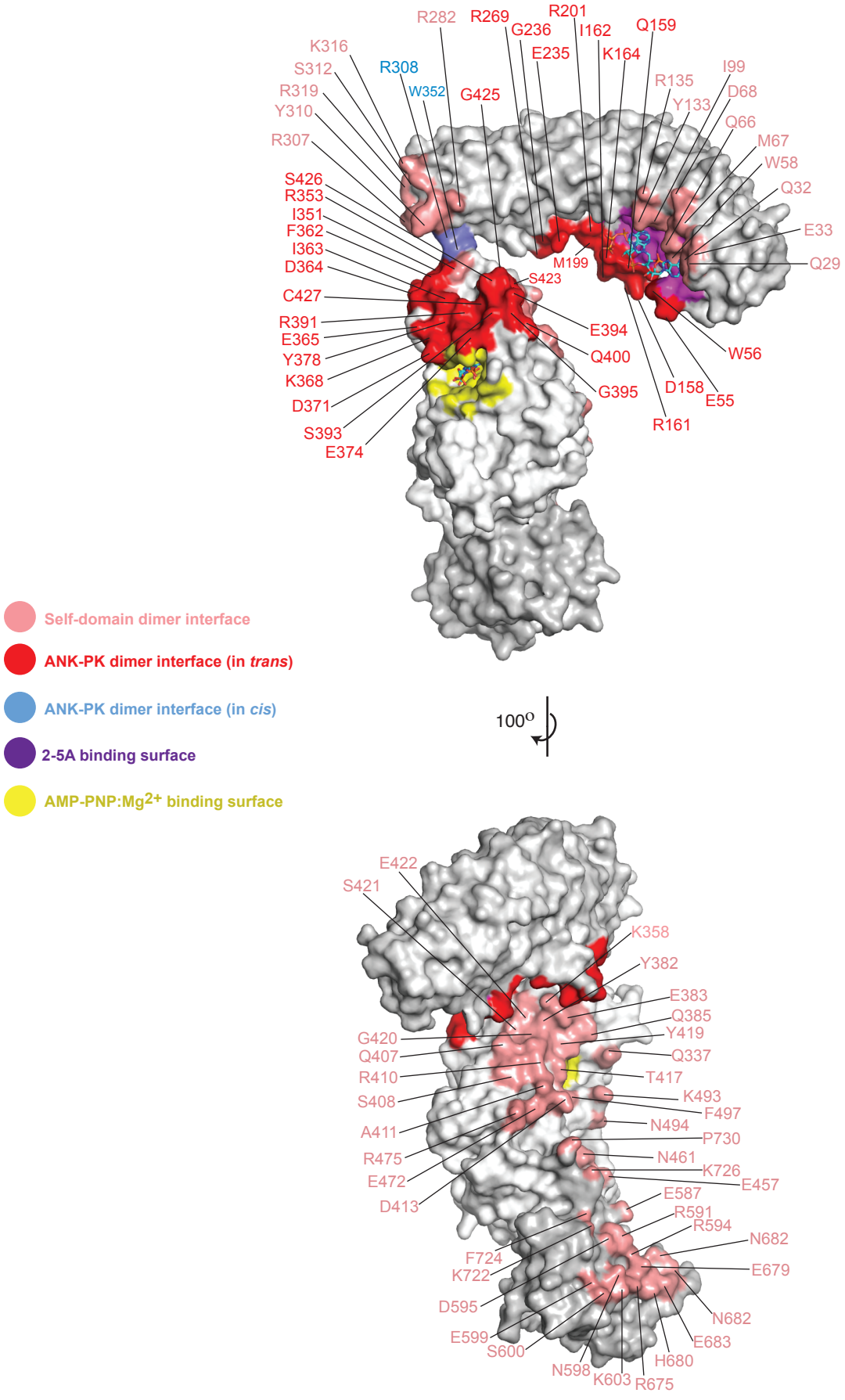

Supplementary Figure 3

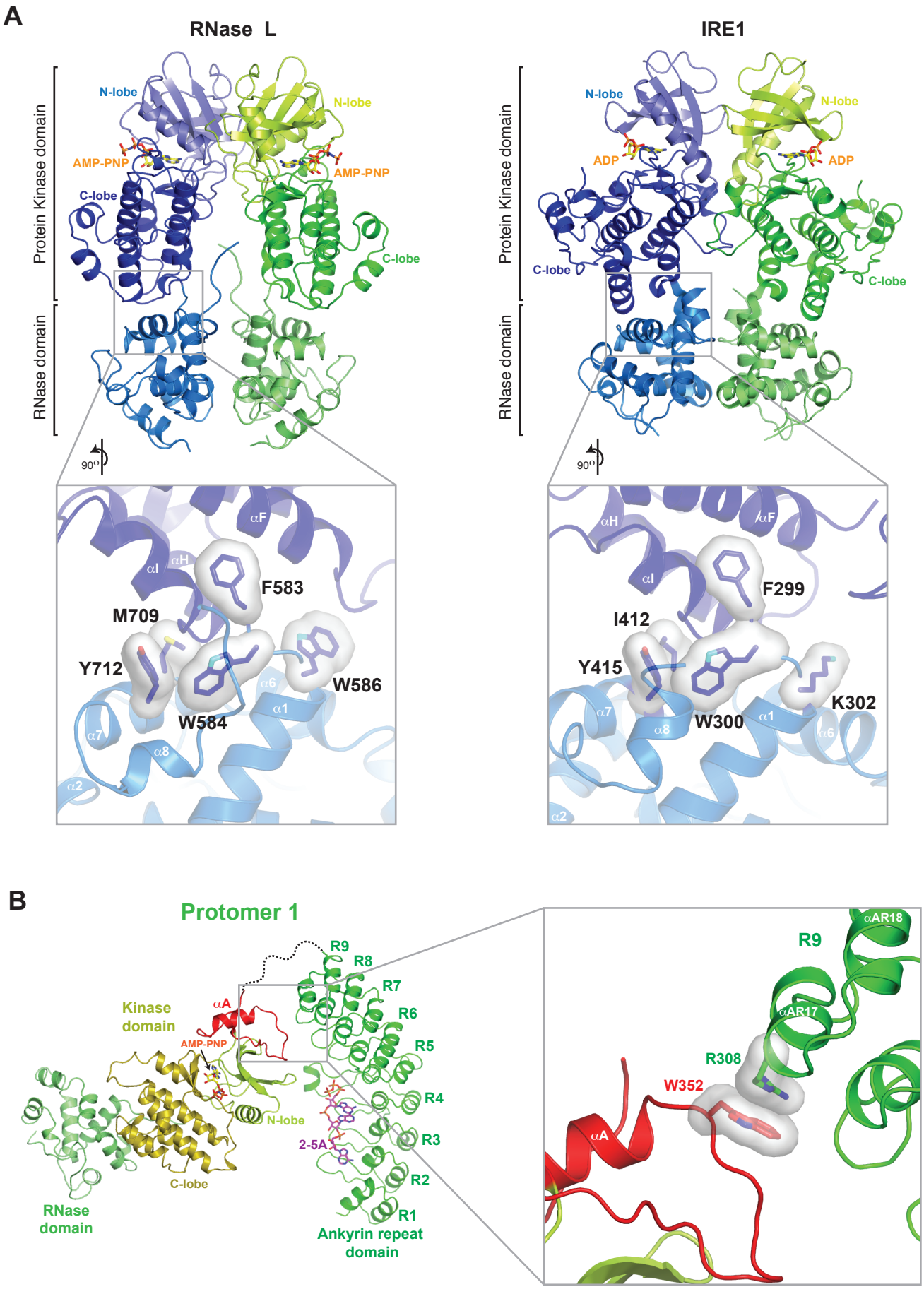

Supplementary Figure 4

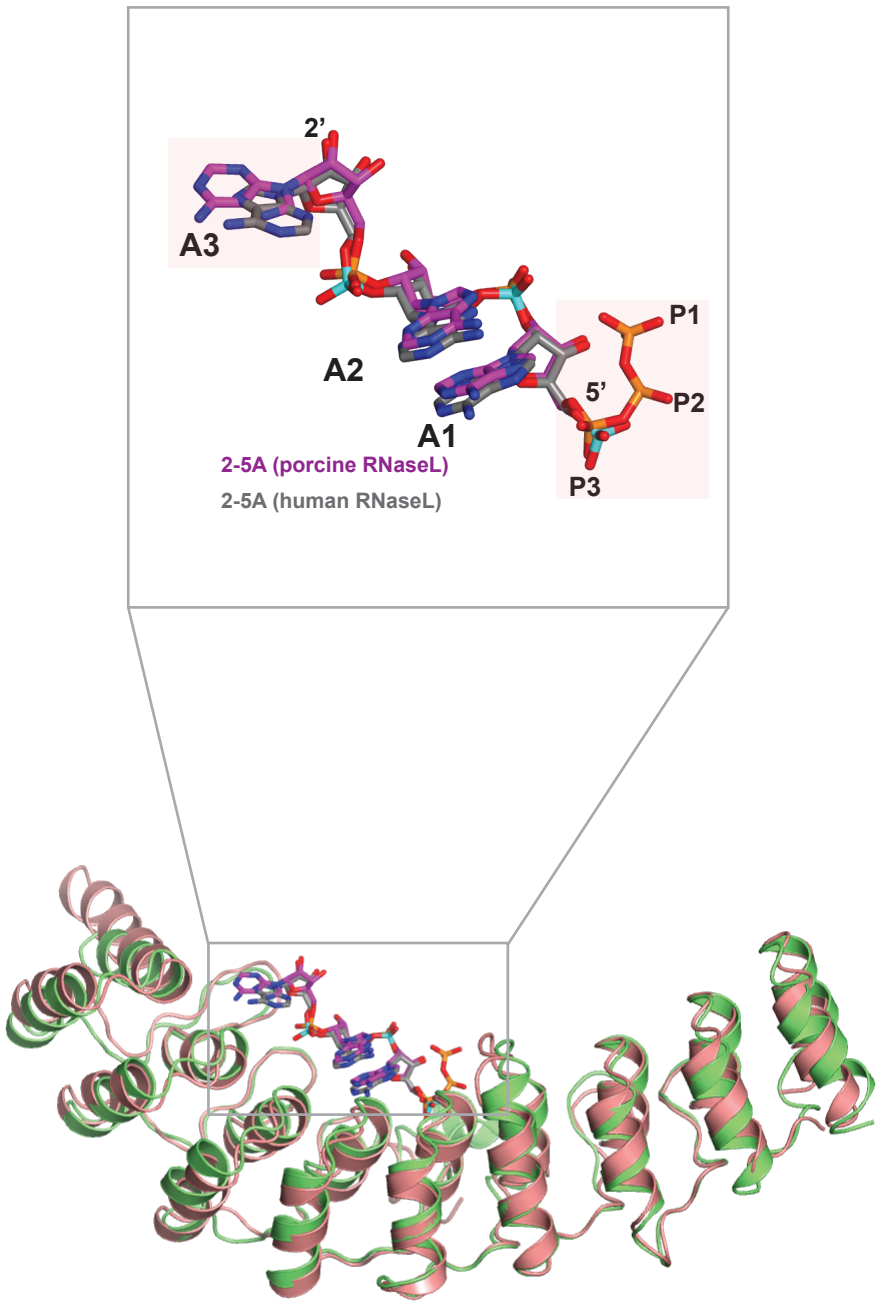

Supplementary Figure 5

A

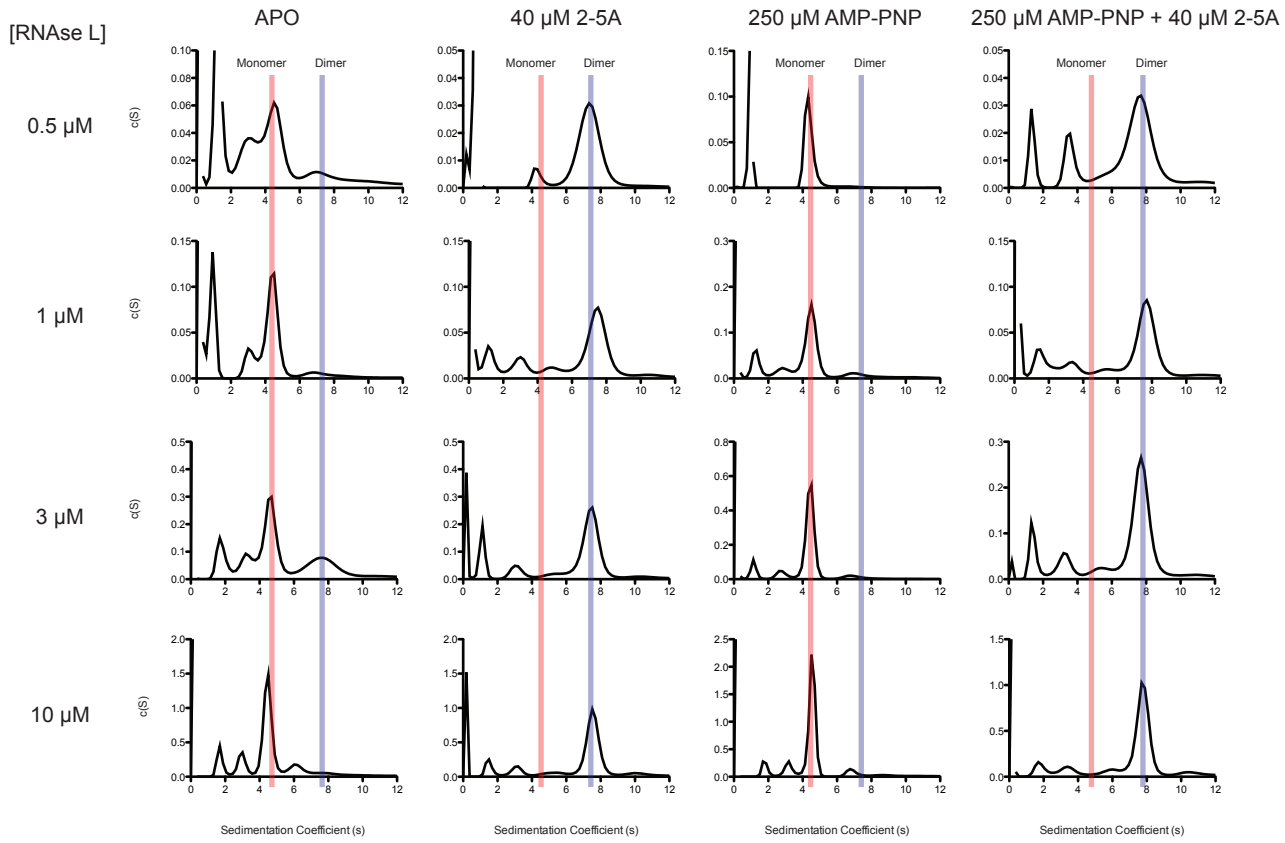

B

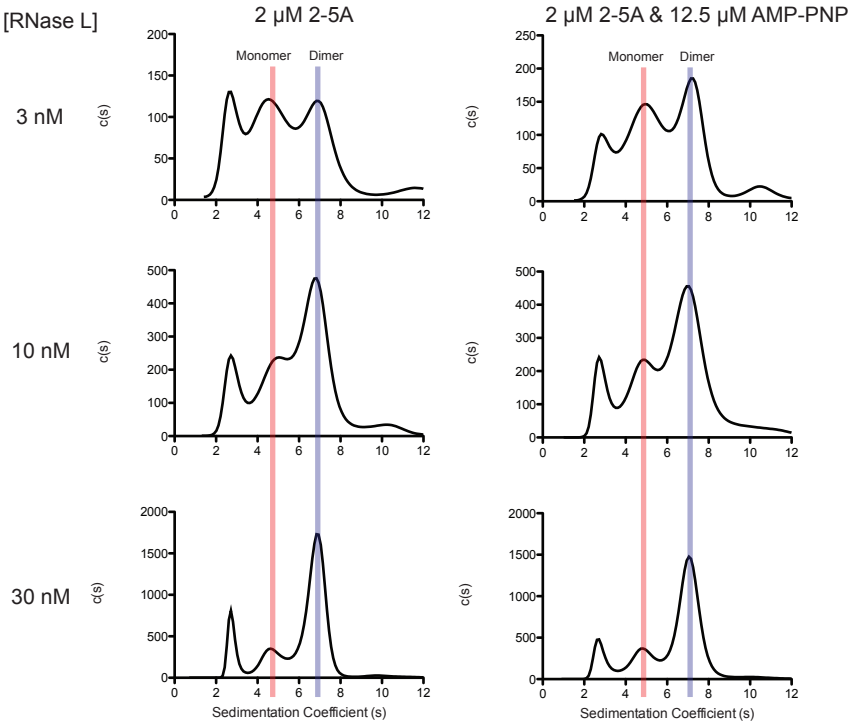

Supplementary Figure 6

A

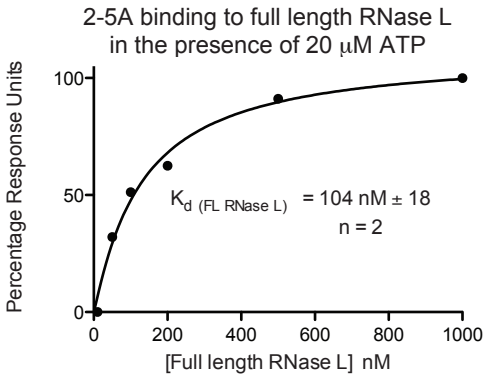

B

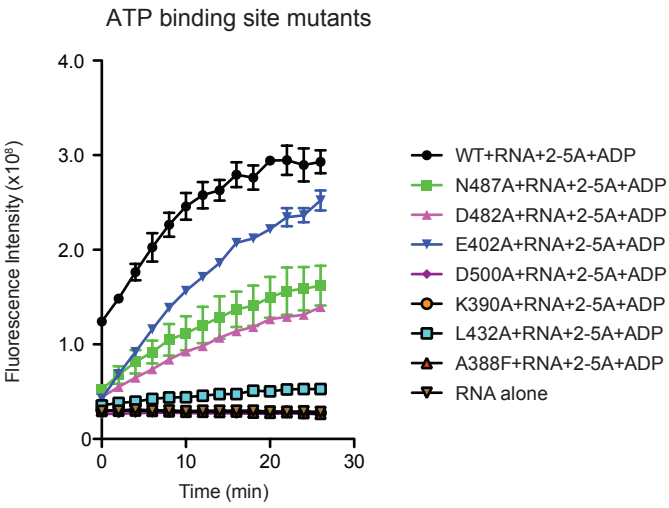

C

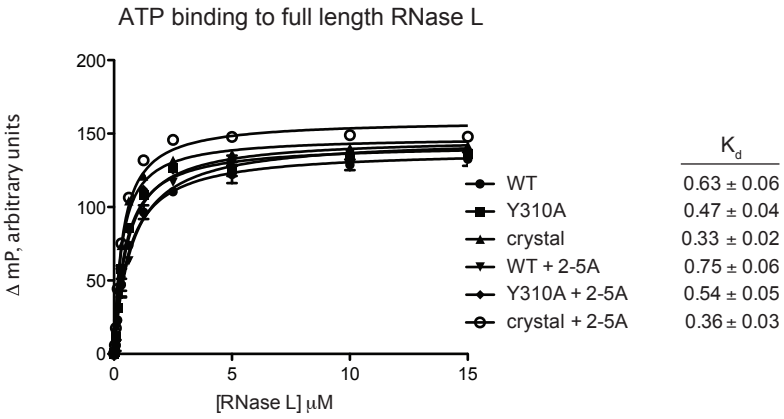

Supplementary Figure 7

SUPPLEMENTARY FIGURE LEGENDS

Figure S1. Representative electron density maps and crystal contacts. Related to Figure 1.
(A) Unbiased F_o-F_c electron density maps (contoured at 2.5σ) centered on the 2-5A **(top panels)** and AMP-PNP **(bottom panels)** ligand binding sites. Maps reflect an atomic model prior to introduction of ligands into the refinement process. Ligands from the final model are shown for comparison. In the absence of electron density for ADP in the ADP free RNase L crystal structure, ADP was not modeled.
(B & C) Packing contacts of RNase L dimers present in the crystal lattice. Protomers within each 2-5A induced dimer are coloured blue and green or red and beige with RNase active sites highlighted by black circle. Inter-dimer contact area = 603 $Å^2$ and 1718 $Å^2$ for (B) and (C), respectively.
(D) Crystal packing contacts of yeast IRE1 dimers implicated in polymer formation (PDBID 3FBV). Protomers within each back-to-back dimer are coloured blue and green or red and beige with RNase active sites highlighted by black circle. Inter-dimer contact area = 2714 $Å^2$.

Figure S2. Sequence alignment of RNase L orthologues and Ire1. Related to Figures 1, 2 and 3.
Structure based multiple sequence alignment of RNase L sequences from *Sus scrofa* (porcine), *H. sapiens* (human), *M. musculus* (mouse), *B. taurus* (cattle), *G. gallus* (chicken) and the dual PK domain – RNase domain module of *S. cerevisiae* (yeast) Ire1 (PDBID 2RIO). The ANK domain, PK domain, and RNase domain regions are highlighted by blue, tan and pink backgrounds. Residues invariant or highly conserved across the RNase L orthologues are shaded black and grey respectively. The secondary structure of *S. scrofa* RNase L is drawn above the alignment. Disordered regions are depicted as dashed lines. Non-canonical features of the pseudokinase domain are highlighted by coloring the secondary structure in red. Conserved RNase domain catalytic residues are colored in purple and key protein kinase catalytic motifs are indicated by magenta-bordered boxes. 2-5A—interacting residues are indicated by stars and AMP-PNP—interacting residues are indicated by grey triangles. Cross-protomer contacts (calculated by AREAIMOL) are indicated by filled boxes colored in green (ANK-PK contacts) and in orange (ANK-ANK, PK-PK or RNase-RNase contacts) boxes above the alignment. Dashed lines represent not modeled disordered regions of the crystal structure.

Figure S3. Contact surfaces between two RNase L protomers. Related to Figure 3.
Surface representation of a single RNase L protomer with dimer interface residues highlighted. Surfaces of atom pairs closer than 5.9 Å are colored as indicated. AMP-PNP and 2-5A are shown as sticks.

Figure S4. Structure analysis of RNase L. Related to Figure 4.
(A) Ribbons comparison of the back-to-back dimer configuration of the dual pseudo PK domain – RNase domain module of RNase L and IRE1. A detailed representation of the

contiguous hydrophobic core linking the protein kinase and RNase domains is shown in the zoom in views below.
(B) Ribbons representation of the tenuous contact between ANK and PK domains within each protomer of a higher order dimer. A detailed representation of interacting residues is shown in the zoom in view to the right.

Figure S5. Structure comparison of ANK domains and 2-5A ligands from isolated ANK and full length RNase L structures. Related to Figure 4.
Cartoon representation of superimposed ANK domains of porcine RNase L and isolated human ANK domain structure (PDBID 4G8L) with bound 2-5A. Bound 2-5A ligands are shown in the zoom in view at top. 2-5A bound to human RNase L (ANK domain alone) is depicted as sticks with grey colored carbons and cyan colored phosphates. 2-5A bound to porcine RNase L is depicted as sticks with magenta colored carbons and orange colored phosphates.

Figure S6. Influence of ligand binding on the oligomerization status of WT porcine RNase L. Related to Figure 5. Analytical ultracentrifugation analyses were performed on (**A**) WT RNase L using refractive index detection or (**B**) fluorescein labeled WT RNase L using fluorescence detection at the indicated protein concentrations with the indicated concentrations of ligands.

Figure S7. In vitro functional characterization of RNase L. Related to Figure 5.
(**A**) Binding of 2-5A to full length RNase L in the presence of 20 μM ADP assessed by surface plasmon resonance. Normalized response levels for specific binding of RNase L to immobilized biotinylated 2-5A were plotted against increasing protein concentration. Reported K_d is the average of two independent experiments (+/- s.e.m). Displayed results are representative of two independent experiments.
(**B**) RNase activity profiles for wild type RNase L and the indicated ATP binding site mutants monitored in the presence of 2-5A activator and 50 μM ATP using a FRET pair labeled RNA substrate. Displayed results are representative of two independent experiments measured in duplicate (+/- s.e.m.).
(**C**) Binding of the fluorescently labeled ATP analogue (BODIPY FL ATP-γ-S) to full length RNase L, a Tyr310Ala mutant, and the crystallization construct (crystal) in the presence and absence of 3 μM 2-5A activator assessed by monitoring the fluorescence polarization signal in the presence of increasing concentrations of protein. Displayed results are representative of two independent experiments measured in duplicate (+/- s.e.m).

Table S1. Small-angle X-ray scattering data collection and analysis. Related to Figure 7.

Ligands	**2-5A**	**2-5A +ADP**
Data-collection parameters		
Instrument	BioSAXS-1000	BioSAXS-1000
Beam geometry (mm)	0.5	0.5
Wavelength (Å)	1.5418	1.5418
q range ($Å^{-1}$)	0.008-0.400	0.008-0.4000
Exposure time (hr)	0.5	2
Concentration (μM)	14	3.9
Temperature (°C)	10	10
Structural parameters		
I_0 (cm^{-1}) [from Guinier]	1.774 ± 0.030	0.1946 ± 0.0136
R_g (Å) [from Guinier]	57.50 ± 1.16	35.7 ± 3.04
Fidelity of Guinier	0.937	0.998
I_0 (cm^{-1}) [from P(r)]	1.642 ± 0.010	0.1975 ± 0.003
R_g (Å) [from P(r)]	55.19 ± 0.256	37.38 ± 0.388
D_{max} (Å)	175	115
Total Quality Estimate [from P(r)]	0.891	0.917
Chi^2 of *Ab Initio* Model	1.17-1.18	0.99

Supplenmentary Experimental Procedures

2-5A synthesis and purification.
2-5A was synthesized as described previously with modifications (Jha et al., 2011). Enzymatic synthesis of 2–5A from ATP was done with recombinant porcine 2'–5' oligoadenylate synthetase (pOAS1) (a gift from Rune Hartmann, Aarhus, Denmark) activated with poly(rI):poly(rC) (pIC) conjugated to CL6B agarose (Ag-pIC). Briefly, pIC was conjugated with CL6B agarose beads (Amersham Biosciences) using per-iodate conjugation chemistry, and Ag-pIC was incubated with 0.4 mg/mL of purified pOAS1 at 25°C in 10 mM HEPES pH 7.5 containing 1.5 mM magnesium acetate, 10% glycerol, 50 mM KCl, and 7 mM β-mercaptoethanol for 1 h. pOAS1 immobilized on Ag-pIC beads was washed three times with buffer and resuspended in the reaction mixture (10 mM ATP, 10 mM magnesium acetate, 20% glycerol, 50 mM KCl, and 7 mM β-mercaptoethanol) for 20 h at 37^{o}C with constant shaking. The unfractionated 2–5A mixture was harvested by centrifugation at 3,000 g for 15 min and then separated from pOAS1with a Centriprep (Millipore) molecular weight cutoff of 3000 Da. The reaction mixture was analyzed on a Dionex PA100 (4 mm x 250 mm) analytical column (Dionex Inc.) interfaced with a System gold HPLC under the control of a 32 Karat work station using $NH_4HCO_3/(NH_4)_2CO_3$ pH 8.0 as mobile phase. The preparative purification of (2'-5')p_3A_3 was done by HPLC on Dionex PA100 (22 mm X250 mm) preparative column by using gradient of 10 mM – 800 mM $NH_4HCO_3/(NH_4)_2CO_3$ pH 8.0 gradient in 70 minutes. The peak fractions were collected and lyophilized (2X in DEPC treated water). The characterization of (2'-5')p_3A_3 (>95% purity) was done by analytical HPLC and ES-MS by direct infusion. The molecular ion was observed at MH_3^+ 1164.23, MH_3^{2+} 581.76 and MH_3^{3+} 387.61. The theoretical molecular weight of (2'-5')p_3A_3 is 1161 Da.

Protein Expression and Purification
Cloning and description of the cDNA for porcine RNase L was described previously (Rios et al., 2007; Zhou et al., 1993)**.** Wild type and mutant *Sus scrofa* RNase L proteins **(**residue 21 to 732 for crystallization studies and residues 1 to 743 for mutational, SAXS and biochemical studies) were recombinantly expressed from a modified pGEX-2T (Pharmacia) plasmid in *E. coli* BL21 cells as TEV protease-cleavable GST-tagged fusions. Bacterial cell pellets were suspended in lysis buffer (30 mM HEPES, pH 7.8, 400 mM NaCl, 2 mM DTT), lysed by homogenization using a cell homogenizer (Avestin Inc.) and centrifuged at 30,000 g for 40 minutes to remove cell debris. Clarified lysate was bound to glutathione Sepharose resin (GE Healthcare) and eluted by TEV protease treatment. Eluate was then purified by anion exchange chromatography (Q-Sepharose^{TM} – GE Healthcare) and finally by size exclusion chromatography using a Superdex^{TM} 200 column (GE Healthcare) equilibrated in 30 mM HEPES (pH 7.8), 100 mM NaCl and 2 mM DTT. Peak protein fractions were pooled and concentrated to 10 to 16 mg/ml (125 to 200 μM) and then flash frozen in liquid nitrogen for long-term storage. RNase L mutants were made using the QuikChange protocol (Agilent) on WT plasmid and verified by DNA sequencing. We note that omission of the ion exchange chromatography step yielded RNase L protein with only a partial dependency of RNase function on nucleotide addition.

Crystallization, Data Collection, and Structure Determination

RNase L protein was labeled with seleno-methionine in BL21 CodonPlus(DE3)-RIL cells (Stratagene) using a published protocol (Van Duyne et al., 1993). Crystals were obtained in 4 μl hanging drops containing an equal volume of protein solution with RNase L (10-14 mg/ml, 125-165 μM), +/- AMP-PNP (300 μM), (2'-5')p_3A_3 (400 μM) and of well solution with 5 mM $MgCl_2$, 5 mM DTT, 18% PEG2000, 100 mM NaCl, and 100 mM SPG buffer, pH 7; $MgCl_2$ was not added for the crystals lacking AMP-PNP. Harvested crystals were cryoprotected with lower well solution. Anomalous dispersion experiment was performed on an AMP-PNP containing crystal on beamline 24-ID (Advanced Photon Source, Argonne, IL). Data was processed with XDS (Kabsch, 2010). An initial electron density map was obtained using a combination of molecular replacement and SAD with Phaser (McCoy et al., 2007) using the human RNase L ANK domain (PDBID 4G8K) as a search model. Density modification was performed using Parrot in CCP4 (1994). The structure was auto-built with Buccaneer (Cowtan, 2006) followed by manual adjustment using COOT (Emsley and Cowtan, 2004). Refinement was performed using REFMAC5 (Murshudov et al., 2011). The structure of crystals grown lacking AMP-PNP was solved by molecular replacement using the AMP-PNP bound model.

Structure analysis and sequence alignments

Multiple sequence alignments were performed using MUSCLE (Edgar, 2004) and displayed, edited and annotated using ALINE (Bond and Schuttelkopf, 2009). Secondary structure was analyzed using DSSP (Kabsch and Sander, 1983) and buried surface area and residue contacts were calculated using the programs AREAIMOL and CONTACT from the CCP4 suite (1994). Structure alignments and structure representations were performed using the PyMOL Molecular Graphics System, Schrödinger, LLC.

Analytical ultracentrifugation

Sedimentation velocity analytical ultracentrifugation was performed with a Beckman ProteomeLab XL-I at 42,000 rpm with either refractive index or fluorescence (Aviv Biomedical Inc.) detector system. Data was obtained over 8 h of centrifugation at 20°C using refractive index detection. Concentrations of RNase L, ranging from 0.5 μM to 10 μM, were analysed in AUC buffer (15 mM Hepes pH 8, 250 mM NaCl, 3 mM DTT, 2.5 mM $MgCl_2$) in the presence or absence of 40 μM 2-5A, 250 μM AMP-PNP, or 250 μM AMP-PNP and 40 μM 2-5A. Concentrations of fluorescein labelled RNase L, ranging from 3 nM to 30 nM, were analysed in AUC buffer in the presence or absence of 2 μM 2-5A, or 12.5 μM AMP-PNP and 2 μM 2-5A. The raw data was analyzed by Sedfit (Schuck et al., 2002) and transformed into a c(s) plot.

Fluorescein labeling of RNase L

A 5 ml reaction volume containing 24 μM purified full length RNase L and 48 μM 2-5A was mixed with 21 μM 5-(and-6)-Carboxyfluorescein, Succinimidyl Ester (5(6)-FAM, SE) (Life Technologies™) in a buffer containing 20 mM HEPES (pH 7.8), 100 mM NaCl, 1 mM DTT and 0.1% DMSO. After incubation at 20 °C for 3 hours shielded from light, labeled protein was separated from free 5(6)-FAM, SE by size exclusion

chromatography. The efficiency of labeling determined by absorbance (ε protein 280 nm = 77810 cm^{-1} M^{-1} ; ε fluorescein 494 nm = 71000 cm^{-1} M^{-1}) was 23%.

Preparation of Conjugate of 2-5A with Biotin

2',5'-tetraadenylate 5'-triphosphate [(2'-5')p_3A_4] was synthesized and purified as described for (2',5')p3A3. The 6-(6-hydrazidohexyl) amidohexyl D-biotinamide was purchased from Dojindo Co. (Kumamoto, Japan). All other reagents were of analytical grade from Sigma-Aldrich (St Louis, Mo USA) and used without any further purification. Hydrazidohexyl-D-biotinamide was linked to (2'-5')p_3A_4 by using periodate conjugation chemistry. Briefly, 5 mM aqueous solution of (2'-5')p_3A_4 was treated with 20 mM $NaIO_4$ on an ice bath for 45 min followed by addition of 50 mM potassium iodide. The resulting precipitate was removed by centrifugation. 6-(6-hydrazidohexyl)amidohexyl D-biotinamide dissolved in dimethylformamide was added to a final concentration of 10 mM to the oxidized (2'-5')p_3A_4 in 20 mM sodium acetate buffer (pH 6.5). The reaction mixture was allowed to proceed on an ice bath with continuous stirring for 60 min. Finally, sodium cyanoborohydride (50 mM final concentration) was added to the reaction mixture and incubated for 90 minutes at 0°C. Formation of the conjugate of (2'-5')p_3A_4 with biotin was validated by HPLC on a Xbridge™ BEH C-18 2.5 µm (2.1 mm x 50 mm) analytical columns (Waters) interfaced with system gold HPLC (Beckmann Coulter Inc). The biotin labelled (2'-5')p_3A_4 was purified by HPLC on a semi preparative Xbridge™ BEH C-18 2.5 µm (4.6 mm x 50 mm) column using mobile phase of (A) (15 mM triethylamin and 400 mM 1,1,1,3,3,3-hexafluoro-2-propanol and (B) methanol gradient (10%-30% in 40min). The conjugate, which eluted at 36 min, was collected and lyophilized, resulting in the purified product (16.4 OD_{260}, yield 40%). The formation of the conjugate was confirmed by ES MS on Quattro Ultima (Micromass) triple quadrupole tandem mass spectrometer. The (2'-5')p_3A_4 -biotin was tested for functional activity in a FRET based RNase L activation assay and used for surface plasmon resonance (SPR) binding analyses.

2-5A binding analysis using surface plasmon resonance (SPR)

SPR studies were performed using a Biacore3000 (Piscataway, NJ). Biotin-labeled 2-5A (10 nM) in buffer A [20 mM Hepes buffer (pH 7.4), 5% (v/v) glycerol, 5 mM $MgCl_2$, 1 mM EDTA, 7 mM 2-mercaptaethanol with 0.005% surfactant P20] was immobilized on streptavidin chips (Biacore SA BR-1003-98) at a flow rate of 10 µl/min for 4 minutes, yeilding 150-160 response units (RU) in the sample cell with buffer A in reference cell. Various concentration of porcine RNase L (0.01 to 5 µM in buffer A either in the absence or presence of 20 µM ATP) was used for binding to chips containing immobilized (2'-5')p_3A_4-Biotin at a flow rate of 20 µl/min for 2.4 min, with a 10 minute stabilization time prior to injection followed by 5 min dissociation in buffer alone. Each concentration was injected in duplicate over all surfaces. Sensograms were analyzed with the BIAevaluation version 3.0. Surface regeneration of chips was achieved by using two pulses of 3 M guanidine-HCl in binding buffer at a flow rate of 50 µl/min for 20 seconds. Non-specific interaction of the analyte and the streptavidin chips were blocked with 50 nM free biotin on both the control as well as the experimental flow channels.

In vitro **RNA cleavage assays**

Methods are essentially as described previously (Thakur et al., 2005) with the following deviations. Reaction volumes were decreased to 30 μL to allow measurement in 384 well micro plates. 2-5A activator, FRET RNA substrate and RNase L proteins were employed at 5 nM, 135 nM, and 1.6 nM respectively and nucleotides were employed at concentrations of 0, 2 or 50μM. Results are representative of minimally two independent experiments performed in duplicate.

Cell Based RNA cleavage assay

The full length (FL) porcine RNase L DNA in pET-M30-2(HTa) was subcloned into pENTR 2B Dual Selection Vector (LifeTechnologies) with BamHI at 5' terminus and XhoI at 3' terminus. The RNase L (FL) cDNA in pENTR 2B was then subcloned into pCS2 (Addgene) mammalian expression vector containing a CMV promoter by LR recombination. Mutants were made with QuikChange II Site-Directed Mutagenesis Kit (Agilent) on WT porcine RNase L and verified by DNA sequencing. The cell based assay for RNase L activity was performed as described previously with modifications (Carpten et al., 2002). HeLa-M cells, deficient in endogenous RNase L, were grown in DMEM with 10% FBS were cultured in 12 well plates ($1x10^5$ per well) for 16 hrs. Cells were transfected with 0.7 μg of the different porcine RNase L cDNAs using Lipofectamine 2000 (LifeTechnologies) for 20 hrs. Subsequently, culture media was replaced for 4 hrs and transfected with 1 μg/well of poly(rI):poly(rC) (Calbiochem) for 3 hrs. Media was removed and total RNA was isolated using Trizol reagent (LifeTechologies) and quantitated by measuring absorbance at 260 nm. RNA, about 0.2 ng per sample, was separated on RNA chips with an Agilent Bioanalyzer 2000. Western blot assays on the transfected cells was determined with monoclonal anti-FLAG antibody and anti-β-actin (Sigma), anti-mouse IgG HRP-linked antibody (Cell signaling) and Western Bright ECL chemiluminescent substrate (Advansta).

SAXS analysis

RNase L (200 μM) was incubated with natural 2-5A ligand (300 μM) in the absence or presence of ADP (300 μM) in 30 mM Hepes pH 8.0, 100 mM NaCl, 2 mM DTT and 5 mM $MgCl_2$, as well as 200 μM ADP for the ADP-bound complex. The RNase L and RNase L-ADP complexes were subsequently resolved over a Superdex-200 (GE Healthcare) size exclusion chromatography column and the homogeneity of the samples was confirmed by dynamic light scattering. The scattering data were collected on a BioSAXS-1000 configured on the right port of a MicroMax-007HF X-ray generator using a 45 μL sample volume. Consecutive scans of 10, 30 and 120 minutes were collected at 10°C over a range of RNase L (1.3-14 μM) and RNase L-ADP (0.7-7.8 μM) concentrations. SAXSLab 3.0.0r1 software (Rigaku) was used to subtract buffer scattering from the protein scattering to generate the sample scattering curves. SAXS profiles were analyzed using the ATSAS program suite (Konarev, 2006). Data quality for different protein concentrations and exposure times was assessed with Kratky plots and screened for aggregation using Guinier Plots. Guinier regions and radius of gyration estimates were derived by the Guinier approximation using the AutoRg function of

Primus (Konarev, 2003). The highest quality estimate as determined by AutoRg and AutoGNOM functions was used to select the samples of RNaseL and RNaseL-ADP that were processed further. Data collection and scattering-derived parameters for the highest quality samples are summarized in **Table S1**. *Ab initio* models were generated using DAMMIF (Franke, 2009) and an averaged model from ten independently generated *ab initio* models was calculated using DAMAVER (Volkov, 2003).

Supplementary Reference List

Bond, C.S., and Schuttelkopf, A.W. (2009). ALINE: a WYSIWYG protein-sequence alignment editor for publication-quality alignments. Acta crystallographica Section D, Biological crystallography *65*, 510-512.

Carpten, J., Nupponen, N., Isaacs, S., Sood, R., Robbins, C., Xu, J., Faruque, M., Moses, T., Ewing, C., Gillanders, E.*, et al.* (2002). Germline mutations in the ribonuclease L gene in families showing linkage with HPC1. Nat Genet *30*, 181-184.

CCP4 (1994). The CCP4 suite: programs for protein crystallography. Acta crystallographica Section D, Biological crystallography *50*, 760-763.

Cowtan, K. (2006). The Buccaneer software for automated model building. 1. Tracing protein chains. Acta crystallographica Section D, Biological crystallography *62*, 1002-1011.

Edgar, R.C. (2004). MUSCLE: multiple sequence alignment with high accuracy and high throughput. Nucleic Acids Res *32*, 1792-1797.

Emsley, P., and Cowtan, K. (2004). Coot: model-building tools for molecular graphics. Acta crystallographica Section D, Biological crystallography *60*, 2126-2132.

Franke, D.a.S., D.I. (2009). DAMMIF, a program for rapid ab-initio shape determination in small-angle scattering. Journal of Applied Crystallography *42*, 342-346.

Jha, B.K., Polyakova, I., Kessler, P., Dong, B., Dickerman, B., Sen, G.C., and Silverman, R.H. (2011). Inhibition of RNase L and RNA-dependent protein kinase (PKR) by sunitinib impairs antiviral innate immunity. J Biol Chem *286*, 26319-26326.

Kabsch, W. (2010). Xds. Acta crystallographica Section D, Biological crystallography *66*, 125-132.

Kabsch, W., and Sander, C. (1983). Dictionary of protein secondary structure: pattern recognition of hydrogen-bonded and geometrical features. Biopolymers *22*, 2577-2637.

Konarev, P.V., Petoukhov, M.V., Volkov, V.V., and Svergun, D.I. (2006). ATSAS 2.1, a program package for small-angle scattering data analysis. Journal of Applied Crystallography *39*, 277-286.

Konarev, P.V., Volkov, V.V., Sokolova, A.V., Koch, M.H.J., and Svergun, D.I. (2003). PRIMUS - a Windows-PC based system for small-angle scattering data analysis. Journal of Applied Crystallography *36*, 1277-1282.

McCoy, A.J., Grosse-Kunstleve, R.W., Adams, P.D., Winn, M.D., Storoni, L.C., and Read, R.J. (2007). Phaser crystallographic software. Journal of applied crystallography *40*, 658-674.

Murshudov, G.N., Skubak, P., Lebedev, A.A., Pannu, N.S., Steiner, R.A., Nicholls, R.A., Winn, M.D., Long, F., and Vagin, A.A. (2011). REFMAC5 for the refinement of macromolecular crystal structures. Acta crystallographica Section D, Biological crystallography *67*, 355-367.

Rios, J.J., Perelygin, A.A., Long, M.T., Lear, T.L., Zharkikh, A.A., Brinton, M.A., and Adelson, D.L. (2007). Characterization of the equine 2'-5' oligoadenylate synthetase 1 (OAS1) and ribonuclease L (RNASEL) innate immunity genes. BMC genomics *8*, 313.

Schuck, P., Perugini, M.A., Gonzales, N.R., Howlett, G.J., and Schubert, D. (2002). Size-distribution analysis of proteins by analytical ultracentrifugation: strategies and application to model systems. Biophys J *82*, 1096-1111.

Thakur, C.S., Xu, Z., Wang, Z., Novince, Z., and Silverman, R.H. (2005). A convenient and sensitive fluorescence resonance energy transfer assay for RNase L and 2',5' oligoadenylates. Methods in molecular medicine *116*, 103-113.

Van Duyne, G.D., Standaert, R.F., Karplus, P.A., Schreiber, S.L., and Clardy, J. (1993). Atomic structures of the human immunophilin FKBP-12 complexes with FK506 and rapamycin. Journal of Molecular Biology *229*, 105-124.

Volkov, V.V.a.S., D.I. (2003). Uniqueness of ab-initio shape determination in small-angle scattering. Journal of Applied Crystallography *36*.

Zhou, A., Hassel, B.A., and Silverman, R.H. (1993). Expression cloning of 2-5A-dependent RNAase: a uniquely regulated mediator of interferon action. Cell *72*, 753-765.